Available online at www.sciencedirect.com
ScienceDirect
Infrared Physics & Technology 49 (2006) 45–52
INFRARED PHYSICS & TECHNOLOGY
www.elsevier.com/locate/infrared

Infrared imaging: Synchrotrons vs. arrays, resolution vs. speed

Erika Levenson [a], Philippe Lerch [b,1], Michael C. Martin [a,*]

[a] *Advanced Light Source Division, Lawrence Berkeley National Laboratory, 1 Cyclotron Road, Berkeley, CA 94720, USA*
[b] *Swiss Light Source, Paul Scherrer Institut, 5232 Villigen, Switzerland*

Available online 10 March 2006

Abstract

At the ALS we have been testing out Thermo-Electron's newest infrared imaging system, the Continuum XL microscope. This microscope is equiped with a 32-element MCT (16 × 2) array which allows rapid infrared imaging with fixed step sizes. The microscope also has a conventional single element MCT-A, which can be swapped for an MCT-B, or InSb detectors. This microscope is installed on ALS Beamline 1.4.4 where the synchrotron source provides high brightness for the single element detectors. We present comparisons of the measured spatial resolutions available with each of these detector types for globar and synchrotron sources as a function of wavelength and optical configuration. We find that the synchrotron retains its superiority for ultimate spatial resolution and signal-to-noise, while the array detection system is fast and convenient for surveying larger regions of a sample. Therefore in practice we use the array system for initial infrared images which allow us to find the regions of interest where we 'zoom in' using the synchrotron source.

Keywords: Synchrotron; Resolution; FTIR; Spectromicroscopy; Array; Imaging; Diffraction

1. Introduction

Synchrotron infrared spectromicroscopy provides diffraction-limited spatial resolution with high signal-to-noise [1,2]. The synchrotron has 100–1000 times higher brightness than a conventional thermal globar source [1–4] enabling a wide variety of new science at small spatial scales [3,4]. A new generation of infrared imaging microscopes employing array detector technology is emerging which can provide higher spatial resolution and significantly increased data acquisition speeds than conventional single detector spectromicroscopy systems [5]. At the advanced light source we have installed one of these newer systems which has dual detectors (single and array) with which we can directly compare the resolution and performance of both sources, both detectors, and a variety of optical configurations. This Thermo-Electron Continuum microscope is installed on Beamline 1.4.4 along with a Thermo-Electron Nexus 870 FTIR bench, while our older single detector microscope remains in active use on Beamline 1.4.3, both operating simultaneously. Both systems have recently been upgraded with new higher speed and higher resolution (0.1 μm) Prior Scientific ProScan II x–y sample stages which increases the convenience for the user, but also allows high-precision resolution and other tests as described here.

Two different spatial resolution tests were performed on a USAF 1951 3-Bar Resolving Test Chart [6] using the mercury cadmium telluride (MCT) array detector with the globar source and the MCT-A* single detector with the synchrotron from ALS Beamline 1.4.4 with both 15× and 32× objectives. The USAF resolution test sample has a metal coating on glass with the resolution test structures patterned into the metal layer. The metal is therefore a high reflectivity sample whereas the glass within the test structures is more absorbing in the infrared. The reflectivity of the glass in the mid-IR is only 15% that of the metal coating. The first spatial resolution test is a step-edge test (also known as a knife-edge test) done by performing a linear scan across the glass to metal interface on a larger square

* Corresponding author. Tel.: +1 510 495 2231; fax: +1 510 495 2067.
E-mail address: MCMartin@lbl.gov (M.C. Martin).
[1] On sabbatical leave at the Advanced Light Source.

1350-4495/$ - see front matter © 2006 Elsevier B.V. All rights reserved.
doi:10.1016/j.infrared.2006.01.026

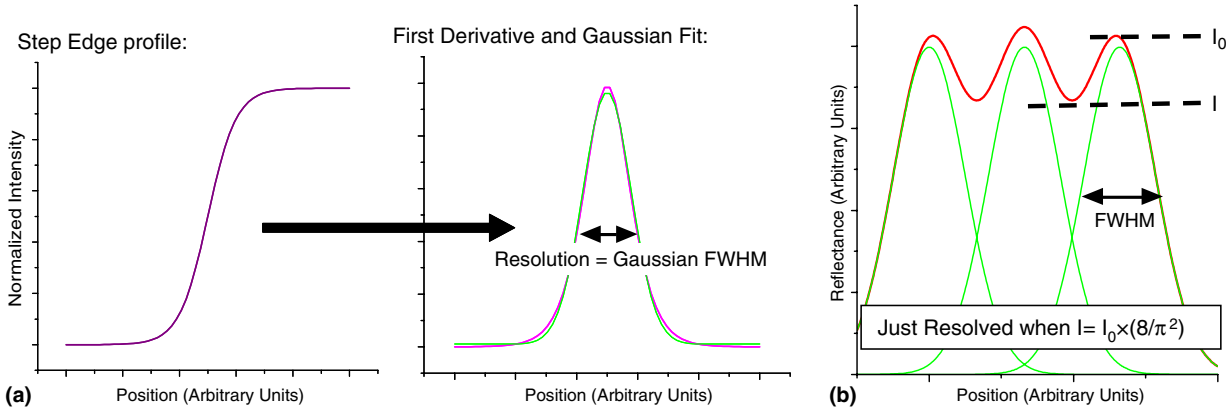

Fig. 1. Resolution test definitions: (a) the step-edge resolution test fits a Gaussian function to the first derivative of the profile. Resolution is given by the FWHM of the Gaussian curve; (b) the imaging resolution test uses Rayleigh's criterion to determine if the peaks are resolved.

portion of the test structure. A spectrum is acquired at each point and then a profile of the reflection as a function of position is obtained. To obtain the resolution, the first derivative of the profile is calculated and then fit to a Gaussian function. The full width half max (FWHM) of the Gaussian fit determines the resolution as shown in Fig. 1(a) [7]. The second type of resolution test, whose definition is shown in Fig. 1(b), is an imaging resolution test done by scanning the beam over three bars of the same width and distance apart. On the USAF test chart there are multiple sets of bars decreasing in width, the smallest being 2.19 μm. Once a reflectance profile is obtained via a line map across a set of three bars, Rayleigh's criterion is used to determine whether the bars are resolved or not. As demonstrated in Fig. 1(b), Rayleigh's criterion states that if the size of the dip between the two peaks overlap (I) is less than $8/\pi^2$ the intensity of the peaks (I_0), then the bars are resolved [8]. These two types of resolution tests were analyzed in order to determine the spatial resolution of the array and synchrotron imaging systems at wavelengths ranging from 1.25 μm to 10 μm (8000–1000 cm^{-1}).

2. Step-edge resolution tests

The first step-edge tests were performed with the 15× and 32× objectives using the array detector. Fig. 2 shows a micrograph of the USAF 1951 3-bar resolving test chart and a close up of the square that was used for the step-edge tests. The red line in Fig. 2 indicates where the line scan was performed over the edge of the square. We analyzed the data at every 1000 wavenumbers from 1000 cm^{-1} (10 μm wavelength) to 6000 cm^{-1} (1.67 μm wavelength). For the 15× objective each array pixel is imaged to 19×17 μm at the sample. Fig. 3(a) shows the edge profiles for each 1000 wavenumbers for the 15× objective. A Gaussian was fit to the first derivative of each profile and the FWHM of the Gaussians is plotted against wavelength in Fig. 3(b). The FWHM is weakly dependent on wavelength and the resolution at each wavelength is approximately twice the pixel size. For the 32× objective each array pixel is imaged to 9×8 μm at the sample. Fig. 3(c) shows the edge profiles for each 1000 wavenumbers and Fig. 3(d) shows the measured Gaussian FWHM vs. wavelength.

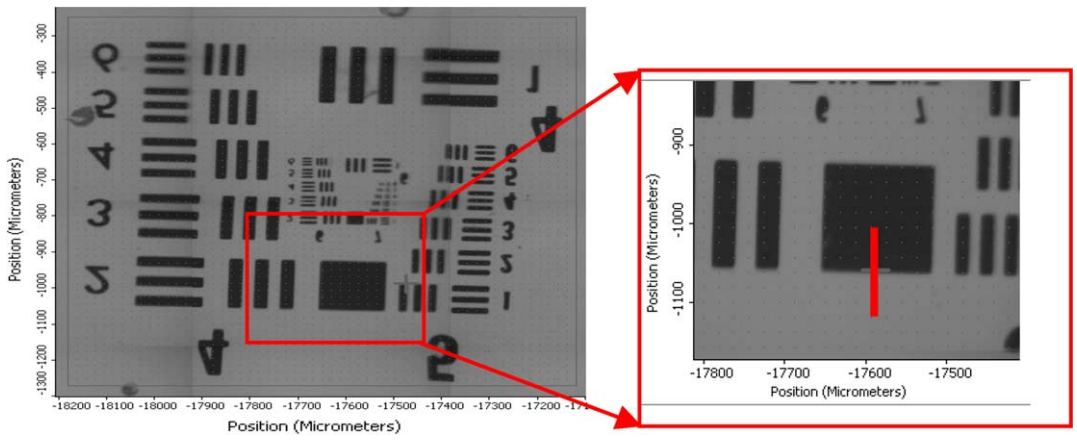

Fig. 2. A micrograph of the USAF 1951 3-bar resolving test chart and a close up of the square that was used for the step-edge tests. The red line indicates where the line scan was preformed over the edge of the square. (For interpretation of the references in colour in this figure caption, the reader is referred to the web version of this article.)

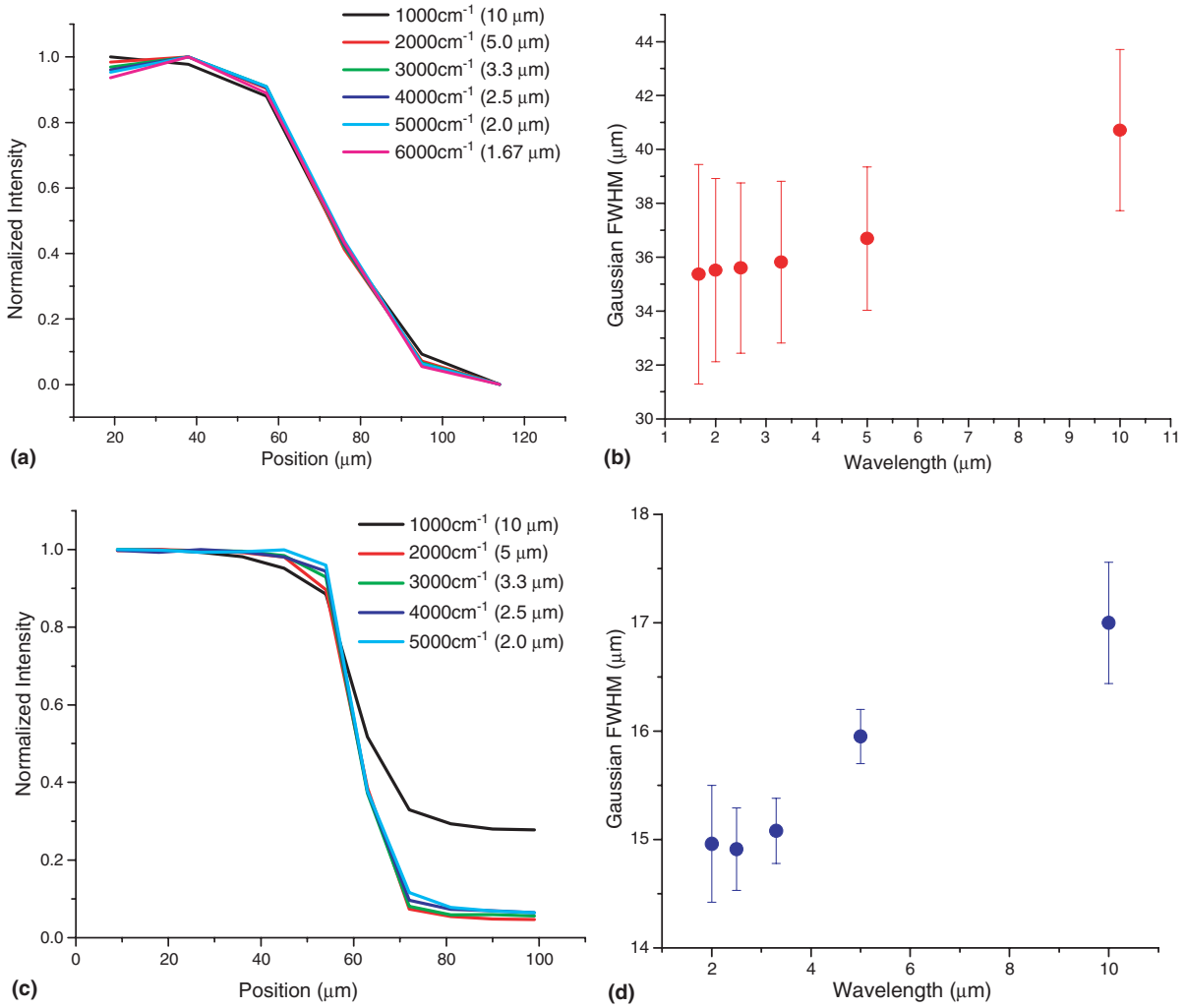

Fig. 3. Step-edge resolution tests using the array: (a) step-edge profiles using the array and the 15× objective; (b) the FWHM of the Gaussians that are fit to the first derivative of the profiles in (a) vs. wavelength; (c) step-edge profiles using the array and the 32× objective; (d) the FWHM of the Gaussians that are fit to the first derivative of the profiles in (c) vs. wavelength.

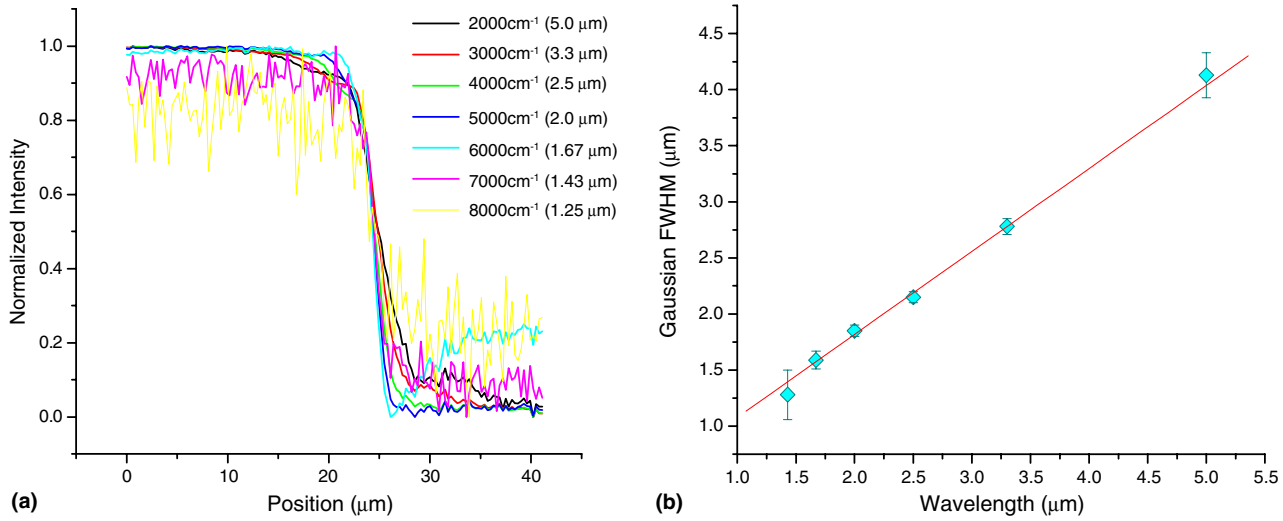

Fig. 4. Step-edge resolution tests with the synchrotron source: (a) step-edge profiles using the synchrotron and the 32× objective; (b) the FWHM of the Gaussians that are fit to the first derivative of the profiles vs. wavelength. The slope of the line gives the resolution for the synchrotron as a function of wavelength.

Again, we find that the resolution of the array is approximately twice the pixel size and only slightly dependent on wavelength.

The next step-edge resolution tests were performed with the 32× using the synchrotron beam and the single detector. Again the analysis was performed every 1000 wavenumbers from 2000 cm^{-1} (5 μm wavelength) to 8000 cm^{-1} (1.25 μm wavelength). The measured profiles are shown in Fig. 4(a) and (b) shows the fitted Gaussian FWHM vs. wavelength together with a linear fit to this data. The slope of the line shows that the resolution for the synchrotron scales with the wavelength, specifically the resolution $= (0.74 \pm 0.04)\lambda$. Similar tests were done with the 32× objective and the synchrotron source and consistent results were found demonstrating that the synchrotron source resolution is only limited by diffraction.

3. Imaging resolution tests

The imaging tests determine the resolution between closely spaced objects and therefore can be a more relevant resolution test for real IR spectromicroscopy applications. Scans were made across bars of decreasing width until the bars could no longer be resolved. For the array data, Rayleigh's criterion analysis was done for 2.5 μm and 5 μm wavelengths. As stated above, with the 15× objective the array pixels are imaged to 19×17 μm. A visual image of the map is shown in Fig. 5(a) and the corresponding infrared image is shown in Fig. 5(b). The red and blue squares indicate which bars the line map was acquired across. The 17.5 μm bars were the last bars to be perfectly resolved by the array at 15×. The next smaller size bars, at 15.6 μm, were not resolved. The profile for the 17.5 μm bars (the red

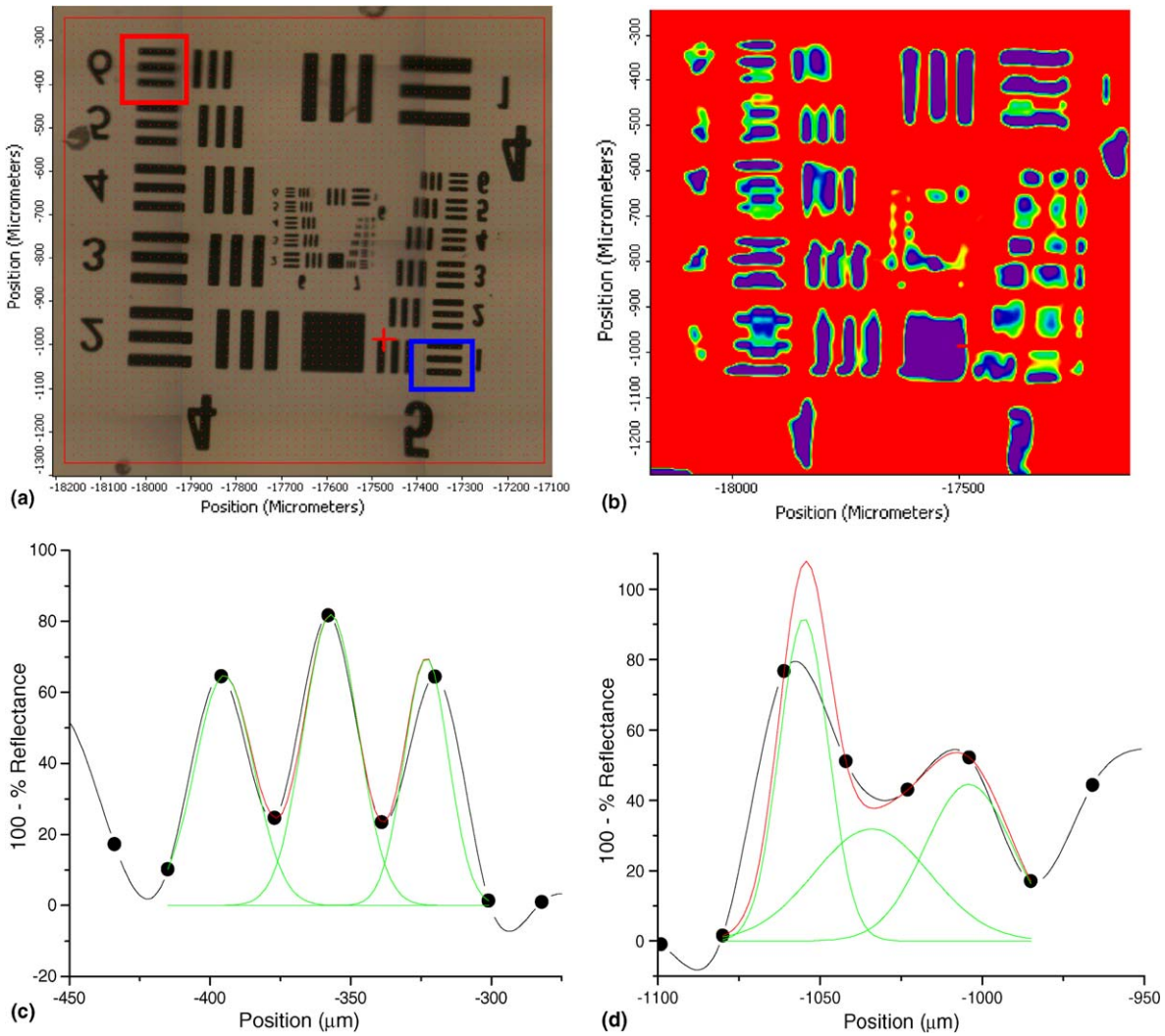

Fig. 5. Imaging resolution tests using the array and the 15× objective: (a) visual image of the test target. The red square outlines the 17.5 μm bars and the blue square outlines the 15.6 μm bars; (b) infrared image of the test target; (c) the profile for the 17.5 μm bars (the red square) at 5 μm wavelength and the Gaussian fits showing these bars are resolved; (d) the profile for the 15.6 μm bars (the blue square) at 5 μm wavelength and the Gaussian fits showing these bars are not resolved. (For interpretation of the references in colour in this figure caption, the reader is referred to the web version of this article.)

square) and 15.6 μm bars (the blue square) at 5 μm wavelength is shown in Fig. 5(c) and (d). The imaging spatial resolution of the microscope at 15× using the array is therefore approximately 17 μm. With the 32× the array pixel is imaged to 9 × 8 μm. A visual image of the map is shown in Fig. 6(a) and the corresponding infrared image is shown in Fig. 6(b). The smallest bar width that was well resolved using the array and the 32× is 9.8 μm. The 8.8 μm bars were just unresolved. The red square in Fig. 6(a) shows the 9.8 μm bars on the map and the blue square shows the 8.8 μm bars. The profiles of these bars at 2 μm wavelength are shown in Fig. 6(c) and (d). The spatial resolution with the 32× is therefore approximately 9.0 μm.

Imaging tests were also done with the synchrotron source with the 15× objective. Analysis based on Rayleigh's criterion was completed for every 1000 wavenumbers from 2000–6000 cm^{-1} (5–1.67 μm) and for 1546 cm^{-1} (6.47 μm). The 3.11 μm bars are just unresolved at 6.47 μm wavelength. The smallest bar resolved at 5 μm wavelength is 2.46 μm. The smallest bar on the test chart, which is 2.19 μm wide, is resolved at all wavelengths shorter than 5 μm. Fig. 7 shows the infrared image of the 2.19 μm bars (a) and the profile of these bars (b) at 2.5 μm wavelength. Since the USAF test chart did not have small enough bars to determine the resolution for wavelengths shorter than 5 μm, we used the measured line widths of the smallest 2.19 μm bars for each wavelength to extrapolate the resolution. By using the Gaussian line widths and Rayleigh's criterion, we can estimate how close together the bars would need to be to no longer be resolved. These extrapolated resolutions, along with the measured resolutions, are shown in Fig. 8. A simple linear relation fits the extrapolated and

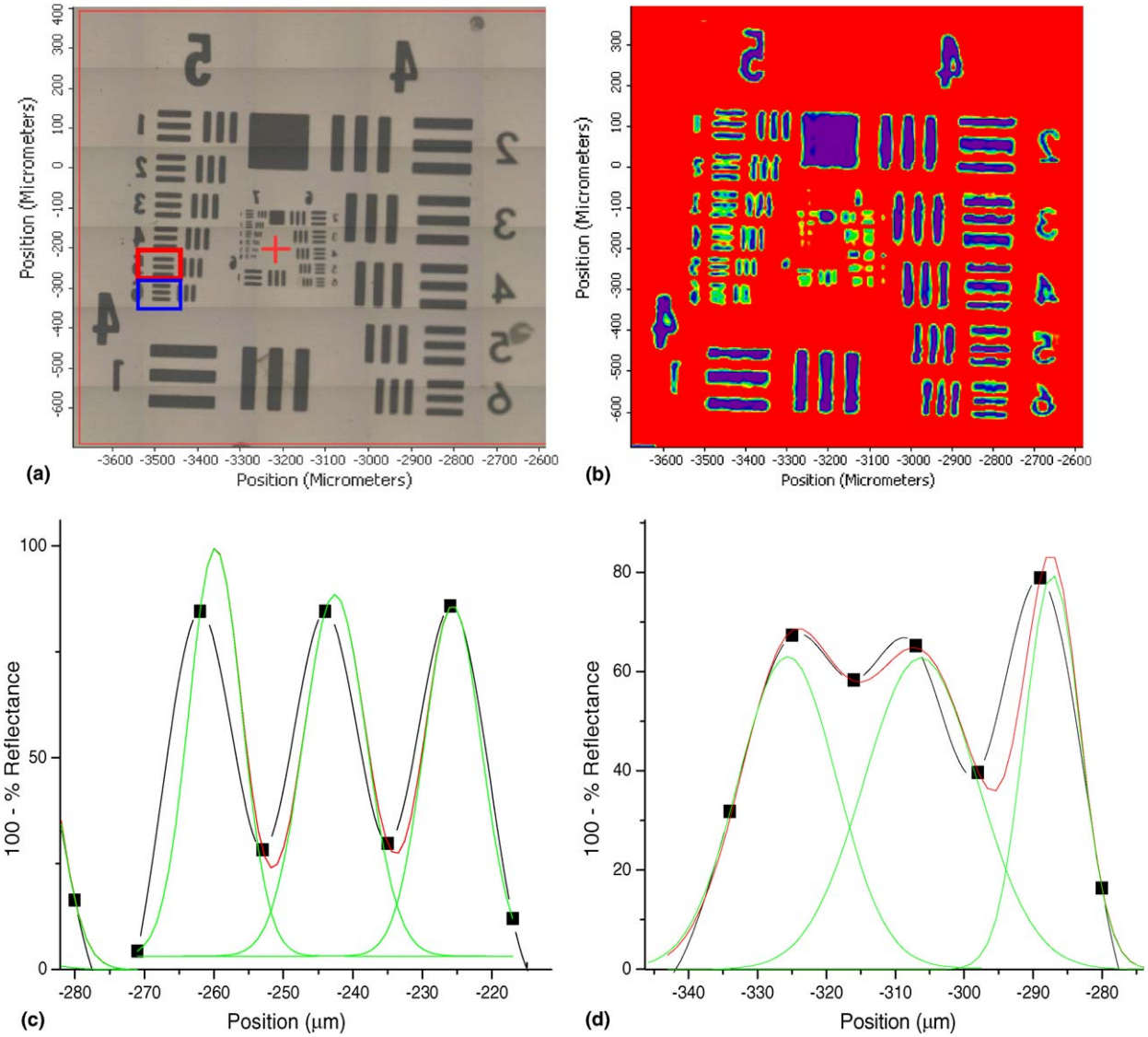

Fig. 6. Imaging resolution tests using the array and the 32× objective: (a) visual image of the test target. The red square outlines the 9.8 μm bars and the blue square outlines the 8.8 μm bars; (b) the infrared image of the test target; (c) the profile and the Gaussian fit for the 9.8 μm bars; the last bars to be well resolved at 2 μm wavelength; (d) the profile and Gaussian fit for the 8.8 μm bars, which are just not resolved. (For interpretation of the references in colour in this figure caption, the reader is referred to the web version of this article.)

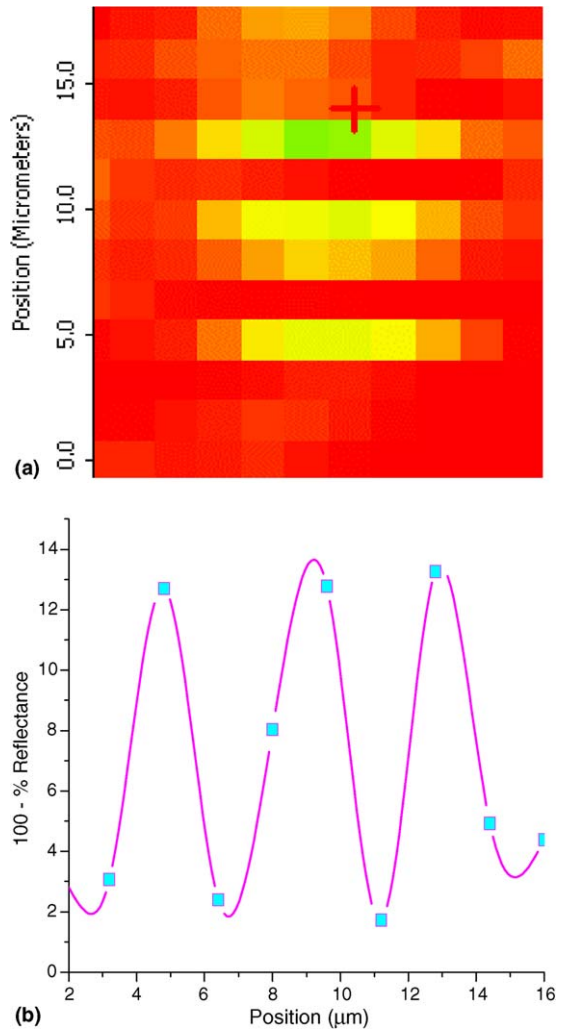

Fig. 7. Imaging resolution tests using the synchrotron and the 15× objective: (a) the infrared image of the smallest 2.19 μm bars at 2.5 μm wavelength; (b) the profile of these bars at 2.5 μm wavelength.

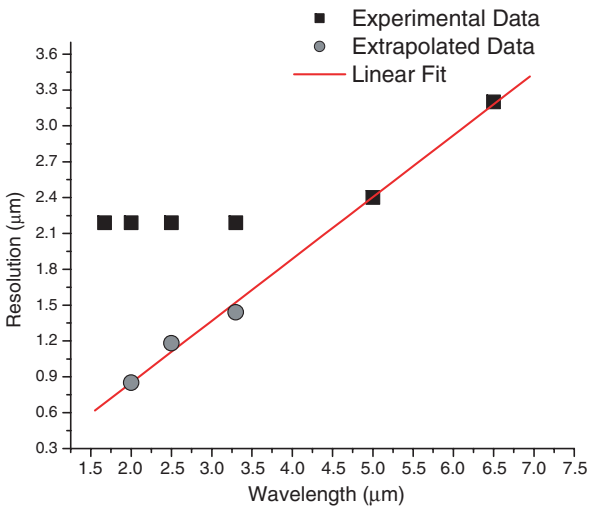

Fig. 8. Extrapolated and measured resolutions vs. wavelength. The dotted line indicates the smallest bar on the test chart. A linear fit of the extrapolated data and the experimental data gives the synchrotron imaging resolution.

measured data points well, resulting in the synchrotron imaging resolution $= (0.52 \pm 0.02)\lambda$.

4. Imaging example

As an example of the imaging capabilities of the array and synchrotron systems, we acquired two spectral images of the same three human cheek cells on a gold coated glass slide. These cells are fairly large in size (~50 μm in diameter) so both imaging systems should be able to easily locate the cells, but finer features such as the nuclei, cellular membranes and cytoplasmic structures will provide a more realistic resolution test. Fig. 9 shows the visual microscope image of the three cells (a), the infrared image of the integrated 2830–3000 cm^{-1} region intensity acquired with the array system (b), and the infrared image of the integrated 2830–3000 cm^{-1} region intensity acquired with the synchrotron source (c). While the three cells are visible with the array system, many finer features are resolved only with the synchrotron source. Fig. 9(d) shows two portions of the spectra obtained from same locations with the two imaging systems. The resolution and acquisition time for the one point were comparable, but we observe that the signal-to-noise ratio of the synchrotron is clearly superior. The array system however retains its speed advantage as its image required only 10 min to acquire while the synchrotron image required over 5 h to complete. The measured S/N for the array is 14 where the S/N for the synchrotron is 4722. The S/N of the synchrotron is therefore about 337 times the S/N of the array. Assuming that noise scales exactly as the in the square root of the number of scans averaged, then 113,000 times more scans are needed with the array to achieve an equivalent S/N as the synchrotron. This means that the acquisition time would be approximately 80 days. This is not very realistic, so another way to compare the S/N of the array and the synchrotron is to calculate the S/N if the array acquired data as long as we took for the synchrotron map (5 h). In this case it would take 1875 scans per pixel in 5 h so the SR would then only have 43 times better S/N than the array, although the resolution superiority of the synchrotron still holds. We therefore find that the array system is excellent at rapidly surveying larger regions of a sample, while the synchrotron is superior for high-quality measurements of small regions at higher resolution and better S/N, in good agreement with Ref. [5].

5. Conclusion

The step-edge resolution tests show that the spatial resolution of the 32-element MCT array is ~2 times the pixel size and only slightly dependent on wavelength, whereas the spatial resolution of the synchrotron is only limited by diffraction at all mid-IR wavelengths. The imaging resolution tests show that the spatial resolution with the MCT array is limited by its projected pixel size whereas the spatial resolution of the synchrotron is again limited by dif-

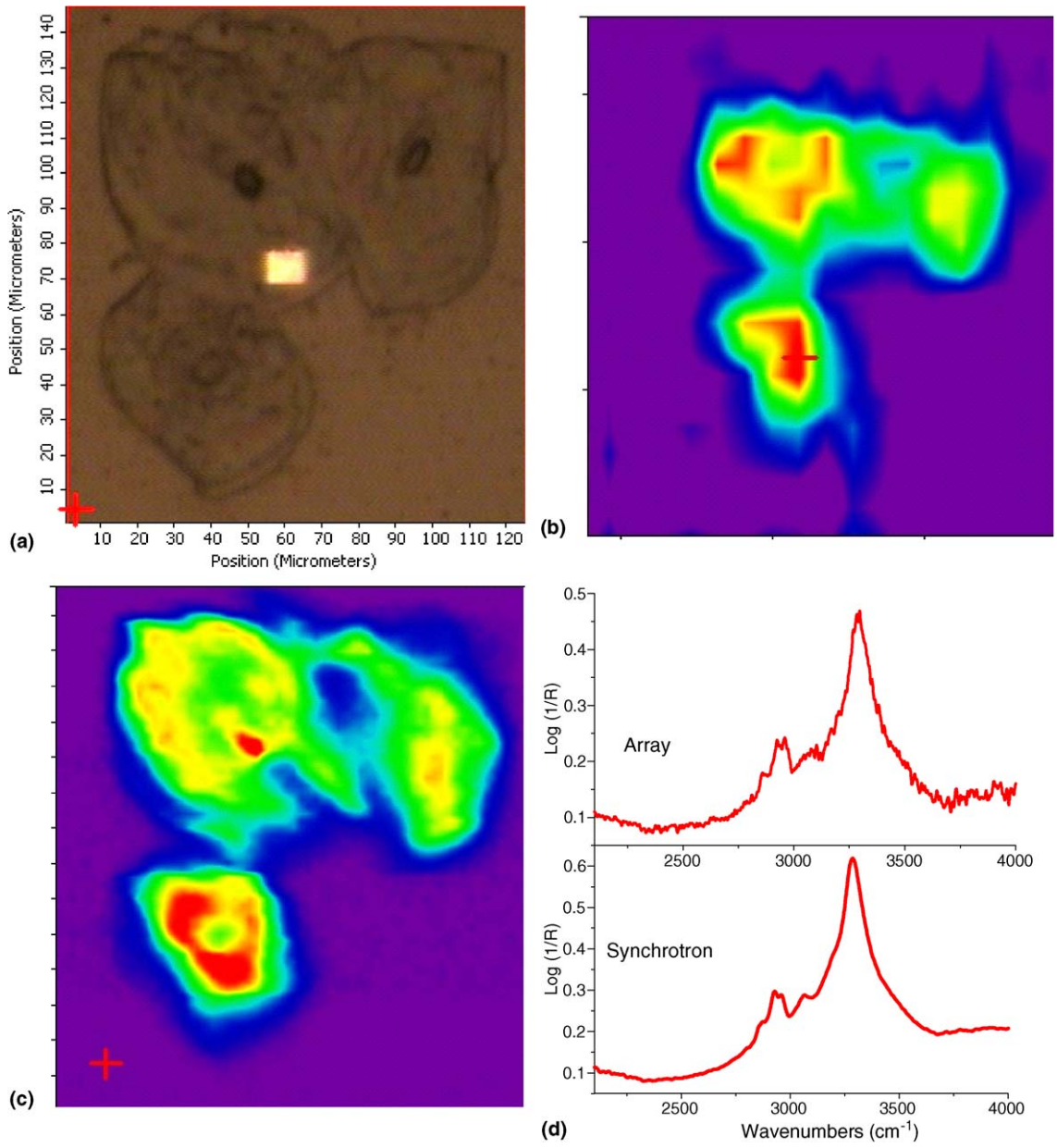

Fig. 9. An example of infrared imaging using human cheek cells: (a) the visual microscope image of the three cheek cells; (b) the infrared image of the integrated 2830–3000 cm^{-1} region intensity acquired with the array system and the 32× objective; (c) the infrared image of the integrated 2830–3000 cm^{-1} region intensity acquired with the synchrotron source; (d) spectra obtained from same locations with the array (top) and the synchrotron (bottom) to demonstrate the signal-to-noise for each system.

fraction at all mid-IR wavelengths and even extending into the near-IR. As array detectors are implemented with effective sizes smaller than the mid-IR wavelengths the spatial resolution of the array will also start to be limited by diffraction. This was not observed in this experiment due to the larger area imaged per pixel size of the MCT array. In both cases the imaging resolution is superior to the resolution determined by the step-edge tests, indicating that features smaller than the measured step-edge resolution may still be resolved in an infrared image.

The MCT Array imaging system is very useful because it multiplexes the data acquisition over 32 elements simultaneously therefore making IR images 32 times faster to acquire. However the spatial resolution is limited by the physical pixel size whereas the synchrotron remains diffraction-limited, has a superior signal-to-noise ratio, and can resolve significantly smaller features. Therefore the synchrotron remains the best tool for the highest spatial resolution with good signal-to-noise. In practice, we use the array system to rapidly image a sample to find the regions of highest interest which are then studied with the synchrotron source at higher resolution. In the future we hope to combine the speed advantages of the array with the quality and resolution of the synchrotron.

Acknowledgements

This work and the Advanced Light Source are supported by the Director, Office of Science, Office of Basic Energy Sciences, Materials Sciences Division, of the US Department of Energy under Contract No. DE-AC03-76SF00098 at Lawrence Berkeley National Laboratory.

References

[1] J.A. Reffner, P.A. Martoglio, G.P. Williams, Rev. Sci. Instrum. 66 (1995) 1298;
G.L. Carr, J.A. Reffner, G.P. Williams, Rev. Sci. Instrum. 66 (1995) 1490;
G.L. Carr, Rev. Sci. Instrum. 72 (2001) 1613.

[2] M.C. Martin, W.R. McKinney, Proc. Mater. Res. Soc. 524 (1998) 11;
M.C. Martin, W.R. McKinney, Ferroelectrics 249 (1–2) (2001) 1–10.

[3] H.-Y.N. Holman, M.C. Martin, W.R. McKinney, Spectrosc—Int. J. 17 (2–3) (2003) 139–159.

[4] P. Dumas, M.J. Tobin, Spectrosc. Eur. 15 (6) (2003) 17–23.

[5] P. Dumas, N. Jamin, J.L. Teillaud, L.M. Miller, B. Beccard, Faraday Discuss. 126 (2004) 289–302.

[6] MIL-STD-150A, Section 5.1.1.7, USAF (1951) 3-Bar Resolving Power Target. Available from: <http://www.efg2.com/Lab/ImageProcessing/TestTargets/>.

[7] J.C. Russ, The Image Processing Handbook, CRC Press, 2002, p. 320.

[8] L. Rayleigh, Phil. Mag. 8 (5) (1879) 261;
E. Hecht, Optics, Addison Wesley Longman, Inc., 1998, p. 416;
M. Born, E. Wolf, Principles of Optics, Cambridge University Press, 1999, p. 371.